Organic LETTERS

Letter

pubs.acs.org/OrgLett

Origin of Kinetic Resolution of Hydroxy Esters through Catalytic Enantioselective Lactonization by Chiral Phosphoric Acids

Avtar Changotra and Raghavan B. Sunoj*

Department of Chemistry, Indian Institute of Technology Bombay, Powai, Mumbai 400076, India

Supporting Information

ABSTRACT: Kinetic resolution is a widely used strategy for separation and enrichment of enantiomers. Using density functional theory computations, the origin of how a chiral BINOL−phosphoric acid catalyzes the selective lactonization of one of the enantiomers of α-methyl γ-hydroxy ester is identified. In a stepwise mechanism, the stereocontrolling transition state for the addition of the hydroxyl group to the *si* face of the ester carbonyl in the case of the *S* isomer exhibits a network of more effective noncovalent interactions between the substrate and the chiral catalyst.

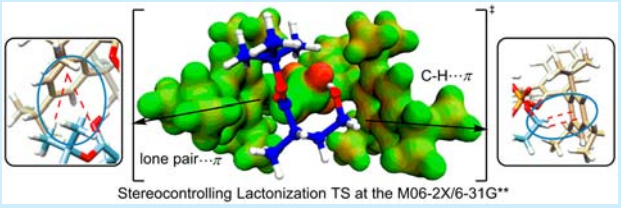

Synthetic protocols to gain access to optically pure compounds have become very timely due to an ever-increasing need for single-enantiomer therapeutics. While the field of asymmetric catalysis offers several ingenious solutions to a desired enantiomer rather directly, reliable techniques for the separation of enantiomers from a racemic mixture have also witnessed considerable advances. Kinetic resolution (KR) offers a distinctive approach for obtaining enantiomerically pure compounds from racemates.[1] Enantioselective transesterification is a commonly employed KR method for the separation of racemic alcohols bearing ester functionality. However, such methods often pose considerable challenges with primary alcohols due to relatively faster lactonization.[2]

Enantioenriched α-substituted γ-hydroxy esters are important building blocks with two diverse functional groups that can be subjected to further synthetic manipulation. Petersen and co-workers recently reported an interesting route toward the synthesis of enantioenriched α-substituted γ-hydroxy esters using KR enabled by chiral Brønsted acid catalysis (Scheme 1).[3] The success of this approach has been attributed to a selective lactonization of one of the enantiomers, which could be traced either to hydrogen bonding or to Brønsted acid catalysis offered by the chiral BINOL−phosphoric acid. The stereochemical outcomes in such reactions are expected to exhibit a pivotal influence on the nature of the substituents on the catalyst, as these reactions take place in the chiral environment provided by the catalyst.[4] Since the pioneering work of Akiyama and Terada, chiral phosphoric acids have emerged as powerful Brønsted acid catalysts with an ever-expanding list of synthetic transformations.[5] The mechanism of action of BINOL−phosphoric acid could vary depending on the class of reaction and the nature of the substrates involved.[6]

Scheme 1. Kinetic Resolution of Hydroxy Ester with Chiral BINOL−Phosphoric Acid (Ref 3)

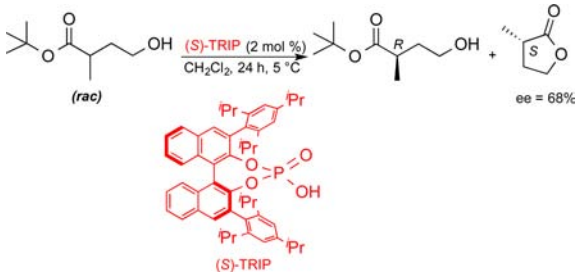

Some of the interesting questions that invite attention are (i) the molecular origin of how (*S*)-TRIP is involved in the selective recognition of one of the enantiomers of the hydroxy ester and converts the same to a lactone and (ii) what are the stereoelectronic features of the transition states that makes the intramolecular lactonization faster when the configuration at the α-carbon of the reactant is *S*? Herein, we employ density functional theory computations at the $SMD_{(DCM)}$/M06-2X/6-31G**//M06-2X/6-31G** level of theory to gain detailed insights into the mechanism and the origin of stereoselectivity of the title reaction. The discussions are presented on the basis of the Gibbs free energies obtained by incorporating the thermal and entropic corrections as obtained at the M06-2X/6-31G** level of theory to the energies in the condensed phase.[7]

The intramolecular lactonization is the key reaction under the chiral environment provided by the BINOL−phosphoric acid. The process can be considered as beginning with the formation of an initial recognition complex between the chiral phosphoric acid and α-methyl γ-hydroxy esters, which will then be followed by an intramolecular nucleophilic attack by the γ-hydroxyl group on the ester carbonyl.[8] Two key modes of Brønsted acid catalysis can be invoked that differ in terms of the site of protonation at the ester group.

Received: June 16, 2016
Published: July 27, 2016

DOI: 10.1021/acs.orglett.6b01752
Org. Lett. 2016, 18, 3730−3733

Protonation at the carbonyl oxygen and at the *tert*-butoxy oxygen are separately considered, as shown in Scheme 2. Since

Scheme 2. Two Likely Mechanistic Possibilities for Lactonization

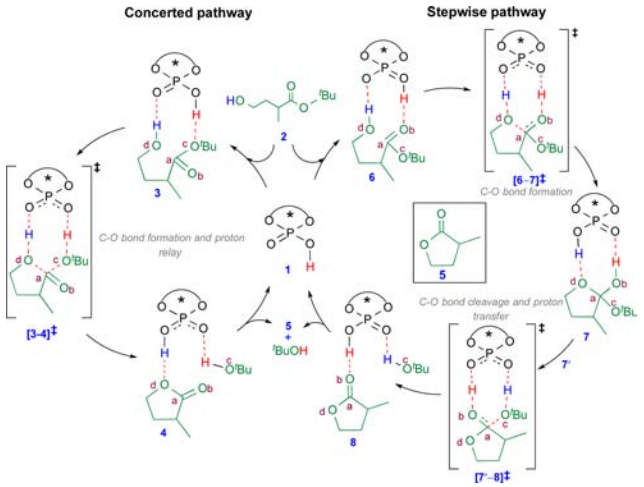

the concerted pathway is expected to be of higher energy (vide infra), herein we focus only on the stepwise mechanism.[9] In the stepwise pathway, the BINOL−phosphoric acid can activate the ester carbonyl group through hydrogen bonding as shown in **6** (Scheme 2). This mode opens up a stepwise pathway via an addition−elimination mechanism. Again, a dual-activation mode is evident, where the ester end of the substrate enjoys a Brønsted acid activation and the hydroxyl group at the other end engages in a hydrogen-bonding interaction with the Brønsted basic oxygen of the catalyst. In such a catalyst−substrate complex, first the nucleophilic attack of the hydroxy group at the electrophilic carbonyl carbon via $[\mathbf{6}-\mathbf{7}]^{\ddagger}$ leads to a tetrahedral intermediate **7**. In the second step, the catalyst helps in the removal of *tert*-butanol by protonating the *tert*-butoxy oxygen via $[\mathbf{7}'-\mathbf{8}]^{\ddagger}$. It is noticed that tetrahedral intermediate **7** undergoes a conformational change to **7′** to enable the protonation at the *tert*-butoxy oxygen.

Although the above-mentioned mechanistic description sounds reasonable, the identification of the lowest energy pathway is a nontrivial exercise. Both the catalyst and the substrate can present a fairly large conformational space owing to the presence of several free rotating bonds. Our ability to ascertain the most preferred mechanistic pathway would therefore demand a detailed conformational sampling. As far as the catalyst framework is concerned, the conformers arising from the rotation of the isopropyl groups are very important. The different conformers of the *p*-isopropyl groups, characterized by two key dihedral angles, Φ_1(H9−C10−C11−C12) and Φ_2(H13−C14−C15−C16), are considered (Figure 1a). In the lactonization transition state, which is the stereocontrolling event, two important conformers of the substrate are considered that differ in the relative orientation of the β-methylene with respect to the ester carbonyl group. The notations *syn* and *anti,* as shown in Figure 1b, respectively, denote that the β-methylene and the carbonyl oxygen are on the same and opposite sides. Nucleophilic addition of the hydroxy group to both the *si* and *re* prochiral faces of the carbonyl group is also considered. The transition states for all these possibilities are separately located, starting from both the *R* and *S* enantiomers of α-methyl γ-hydroxy ester.

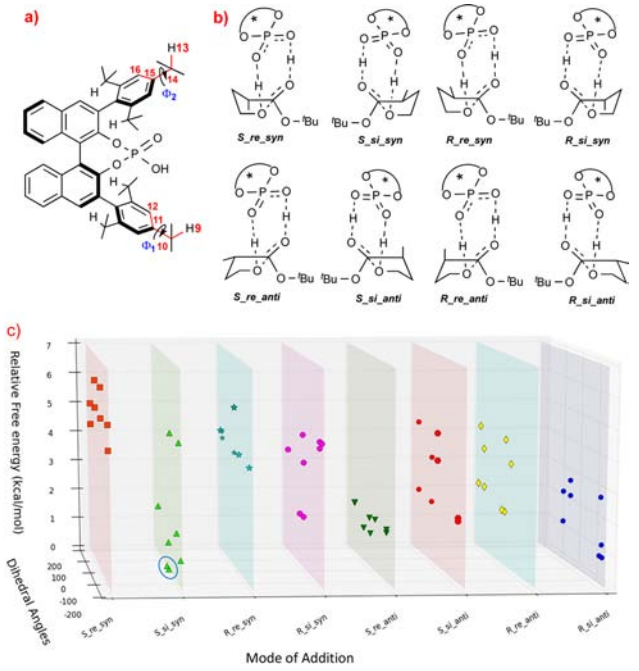

Figure 1. (a) Key dihedral angles Φ_1 and Φ_2 employed in the conformational sampling. (b) Different conformers of the transition states for *S* and *R* enantiomers of the substrate in the stepwise pathway. (c) Gibbs free energies (kcal/mol) of various conformers of these transition states.

Different conformational possibilities and the corresponding spread in the transition-state energies are depicted in Figure 1c. A total of 32 transition states are grouped into eight vertical panels in this figure. Each panel corresponds to a particular group of transition states that belongs to a given configuration of the substrate (*R* or *S*), wherein hydroxy group adds to the *si* or *re* prochiral face of the ester carbonyl with a *syn* or *anti* orientation of the β-methylene. It can be noticed that the lowest energy transition state in the case of *S* hydroxy ester (the second vertical panel from the left) is when the addition to the *si* face of the ester takes place with a *syn* orientation of the β-methylene group. Inspection of the right most vertical panel conveys that the most preferred mode of addition in the case of *R* hydroxy ester is through the *si* face with an *anti* orientation of the β-methylene group.

The lowest energy transition state, obtained through a rigorous analysis of various possibilities in each of the stereochemical modes of addition of the hydroxyl group to the *si* and the *re* faces of the ester, is henceforth considered for more discussions.[10] The activation barrier for the stepwise pathway is found to be 10.8 kcal/mol lower than for the concerted pathway. The lowest energy $[\mathbf{6}-\mathbf{7}]_{S\_si\_syn}^{\ddagger}$, wherein the hydroxy group adds to the *si* face of the ester carbonyl corresponds to the *S* enantiomer of the final product lactone. Transition state $[\mathbf{6}-\mathbf{7}]_{S\_si\_syn}^{\ddagger}$ with dihedral angles of Φ_1 −12.0° and Φ_2 17.2° leading to *S* lactone is found to be 0.9 kcal/mol lower than the diastereomeric $[\mathbf{6}-\mathbf{7}]_{R\_si\_anti}^{\ddagger}$ leading to *R* lactone. This energy difference corresponds to an enantiomeric excess of 64% in favor of the *S* enantiomer of the product lactone, which is in agreement with the experimental value of 68%.[3] The activation barrier for $[\mathbf{6}-\mathbf{7}]_{S\_si\_syn}^{\ddagger}$ is 1.9 kcal/mol lower than that for $[\mathbf{6}-\mathbf{7}]_{R\_si\_anti}^{\ddagger}$ in the stepwise pathway.[11] The enantiomeric excess for unreacted starting material, i.e., α-methyl γ-hydroxy ester, is computed as 46%, again quite comparable to the experimental

DOI: 10.1021/acs.orglett.6b01752
Org. Lett. 2016, 18, 3730−3733

value of 57%.[12] Further rationalization of the energy difference between $[\mathbf{6}-\mathbf{7}]_{S\_si\_syn}^{\ddagger}$ and $[\mathbf{6}-\mathbf{7}]_{R\_si\_anti}^{\ddagger}$ is done by activation strain analysis.[13] The destabilizing distortion of the substrate and the catalyst is found to be more in the higher energy $[\mathbf{6}-\mathbf{7}]_{R\_si\_anti}^{\ddagger}$. Interestingly, the stabilizing interaction energy between the substrate and the catalyst is found to be higher in $[\mathbf{6}-\mathbf{7}]_{S\_si\_syn}^{\ddagger}$. However, the overall balance between distortion and interaction is in favor of the lower energy $[\mathbf{6}-\mathbf{7}]_{S\_si\_syn}^{\ddagger}$ by 0.5 kcal/mol.

After having identified the stereocontrolling transition states, we probed the difference in the intramolecular interactions that renders $[\mathbf{6}-\mathbf{7}]_{S\_si\_syn}^{\ddagger}$ relatively more stabilization over the diastereomeric $[\mathbf{6}-\mathbf{7}]_{R\_si\_anti}^{\ddagger}$. As the first step in this direction, the optimized geometries of the stereocontrolling C−O bond formation transition states, presented in Figure 2, are carefully

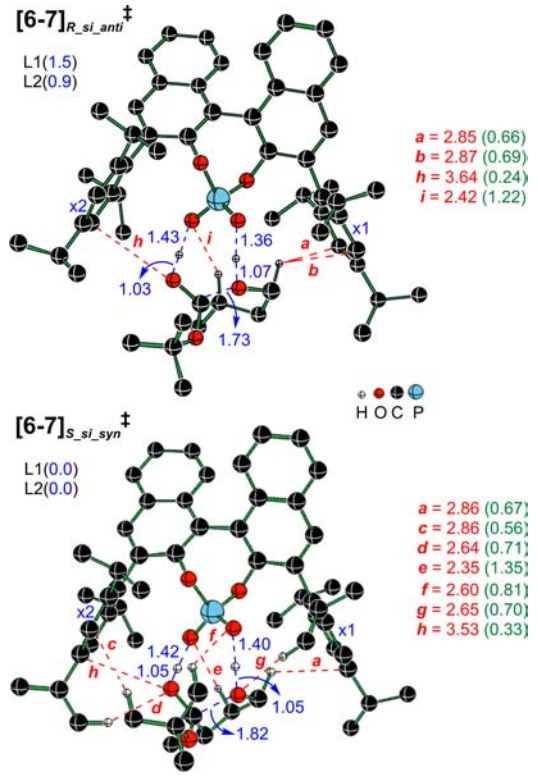

Figure 2. Stereocontrolling transition states for the C−O bond formation at the M06-2X/6-31G** level of theory (L1). Single-point energies at the $SMD_{(DCM)}$/M06-2X/6-31G**//M06-2X/6-31G** (L2). Interatomic contacts shown in red are in angstroms and the corresponding electron densities ($\rho \times 10^{-2}$) at the bond critical points as obtained through AIM analysis are given in parentheses in green. Only selected hydrogens are shown for improved clarity.

analyzed. A comparison of the geometrical features reveals that the stabilization of these transition states appears to depend on the relative stereochemical disposition between the α-methyl group and the *tert*-butoxy group in addition to the difference in the series of noncovalent interactions between the catalyst and the substrate.

We notice that the number and the nature of such weak interactions are different in both the stereocontrolling transition states. To identify the presence of these interactions, we have employed two topological methods based on electron densities; namely, the atoms-in-molecule (AIM)[14] and noncovalent interactions (NCI) plots. The topological distribution of the electron density revealed the presence of bond paths connecting the interacting atoms, and the corresponding electron densities at the bond critical points are provided in parentheses beside each interatomic contact distances in Figure 2. The triisopropyl aryl groups attached to the 3,3′ positions of BINOL-phosphoric acid is denoted as x1 and x2 in Figure 2.

The lowest energy transition state $[\mathbf{6}-\mathbf{7}]_{S\_si\_syn}^{\ddagger}$ enjoys additional C−H···π (*c*) and C−H···O (*d*, *e*, *f*, *g*) interactions compared to those present in the corresponding higher energy diastereomeric transition state $[\mathbf{6}-\mathbf{7}]_{R\_si\_anti}^{\ddagger}$. The efficiency of the common interaction, such as C−H···π (*a*) between the methylene hydrogen of the substrate and the aryl ring of the catalyst (x1), is found to be very similar. The other weak interactions such as the lone pair···π (*h*) between the carbonyl oxygen and aryl ring of the catalyst (x2) and C−H···O (*e*) between the methylene hydrogen and the oxygen of the BINOL−phosphoric acid are also shorter in the lower energy $[\mathbf{6}-\mathbf{7}]_{S\_si\_syn}^{\ddagger}$ than that in the higher energy $[\mathbf{6}-\mathbf{7}]_{R\_si\_anti}^{\ddagger}$. The ρ_{bcp} values for C−H···π, C−H···O, and lone pair···π interactions are, respectively, in the range of 0.0056−0.0069, 0.0069−0.0135, and 0.0024−0.0033, which is characteristic of weak noncovalent interactions.[15] The presence of more number of C−H···π and C−H···O interactions are identified as vital to the differential stabilization of the lower energy transition state. There has been increasing emphasis in the recent years on the role of weak noncovalent interactions in stereocontrolling transition states.[16]

Establishing the presence of weak noncovalent interactions (NCI) in a given transition states is not always an easy task. Recently, Yang and co-workers introduced a valuable graphical tool, termed as NCI plot, primarily to identify the regions of noncovalent interactions by using reduced density gradient isosurface.[17] Such analysis can locate the region and strength of noncovalent interactions. The NCI plots for the stereocontrolling transition states are provided in Figure 3. In an

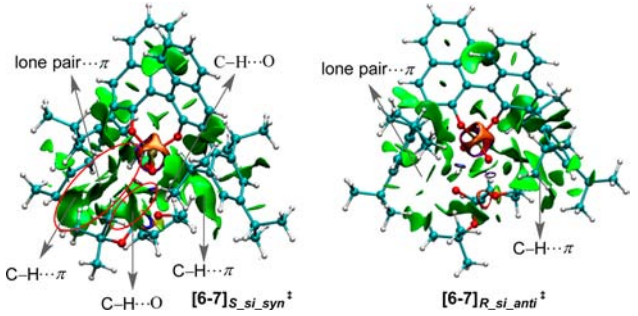

Figure 3. Noncovalent interaction analysis (blue, strong attraction; green, weak interaction; and red, strong repulsion) for stereocontrolling transition states $[\mathbf{6}-\mathbf{7}]_{S\_si\_syn}^{\ddagger}$ and $[\mathbf{6}-\mathbf{7}]_{R\_si\_anti}^{\ddagger}$.

NCI plot, strong attractive interactions appear as blue regions, weak noncovalent interactions as green regions, and repulsive interactions as red regions. It can be noticed that the green regions of weak noncovalent interactions are more widespread and relatively more prominent in the lower energy $[\mathbf{6}-\mathbf{7}]_{S\_si\_syn}^{\ddagger}$. For additional attention, some regions are encircled where dominant noncovalent interactions are noticed. The most important noncovalent interactions are between the aromatic π face of the aryl arm of the catalyst with (a) *tert*-butoxy hydrogen and (b) the carbonyl oxygen of the substrate. In addition, the phosphate oxygen of the catalyst engages in a hydrogen bonding interaction with the *tert*-butoxy hydrogen of the substrate. These critical weak interactions are either absent or diminishingly lower

DOI: 10.1021/acs.orglett.6b01752
Org. Lett. 2016, 18, 3730−3733

in the higher energy transition state $[\mathbf{6}-\mathbf{7}]_{R\_si\_anti}^{\ddagger}$. Additional weak interactions such as C−H···O and C−H···π interactions offered by the other aromatic ring of the catalyst can also be noticed in the NCI plots. Interestingly, the bond critical points obtained through AIM topological analysis exhibits a good correlation with the insights gathered through the NCI plots.

Comparison of the NCI plots for the diastereomeric transition states (Figure 3) provides a clear and distinguishable difference in the pattern of noncovalent interactions. Such differences are the most vital contributing factor to the energy difference between $[\mathbf{6}-\mathbf{7}]_{S\_si\_syn}^{\ddagger}$ and $[\mathbf{6}-\mathbf{7}]_{R\_si\_anti}^{\ddagger}$ and hence responsible for the stereochemical course of the reaction.

These molecular insights could provide leads for catalyst design. The 3,3′-aryl groups on the BINOL framework plays an important role in placing the substrate in a manner that one of the prochiral faces of the ester carbonyl is more preferred for lactonization.[18] Since the C−H···π interactions are found to be important, such substitutions are also expected to influence the energetic preferences. For instance, the introduction of an additional phenyl group at the chiral center of the substrate is predicted to yield higher enantioselectivity as it can participate in more C−H···π interactions with the catalyst.

In summary, the most preferred transition state in Brønsted acid catalyzed kinetic resolution of α-methyl γ-hydroxy esters involves a dual activation mode wherein the BINOL−phosphoric acid promotes an enantioselective lactonization of one of the enantiomers over the other through a stepwise addition−elimination pathway. In the key lactonization transition state, the hydroxyl group from one end of the reactant adds to the *si* face of the ester carbonyl at the other end leading to the preferential formation of the *S* enantiomer of the lactone. A network of favorable noncovalent interactions (such as C−H···π, C−H···O, and lone pair···π) between the substrate ester and catalyst BINOL-phosphoric acid is noticed in the lower energy transition state. The 3,3′-aryl groups of the catalyst controls the orientation of the substrate within the chiral pocket of the BINOL−phosphoric acid.

■ ASSOCIATED CONTENT

Supporting Information

The Supporting Information is available free of charge on the ACS Publications website at DOI: 10.1021/acs.orglett.6b01752.

Optimized geometries, details of conformational analyses, and AIM data (PDF)

■ AUTHOR INFORMATION

Corresponding Author

*E-mail: sunoj@chem.iitb.ac.in.

Notes

The authors declare no competing financial interest.

■ ACKNOWLEDGMENTS

Computing time from IIT Bombay supercomputing and a senior research fellowship from UGC-New Delhi (A.C.) are acknowledged.

■ REFERENCES

(1) (a) Gurubrahamam, R.; Cheng, Y.-S.; Huang, W.-Y.; Chen, K. *ChemCatChem* **2016**, *8*, 86. (b) Dong, S.; Frings, M.; Cheng, H.; Wen, J.; Zhang, D.; Raabe, G.; Bolm, C. *J. Am. Chem. Soc.* **2016**, *138*, 2166. (c) Lorenz, H.; Seidel-Morgenstern, A. *Angew. Chem., Int. Ed.* **2014**, *53*, 1218. (d) Sakuma, M.; Sakakura, A.; Ishihara, K. *Org. Lett.* **2013**, *15*, 2838. (e) Yang, X.; Bumbu, V. D.; Birman, V. B. *Org. Lett.* **2011**, *13*, 4755. (f) Coric, I.; List, B. *Nature* **2012**, *483*, 315. (g) Wang, M.; Huang, Z.; Xu, J.; Chi, Y. R. *J. Am. Chem. Soc.* **2014**, *136*, 1214. (h) Kuwano, S.; Harada, S.; Kang, B.; Oriez, R.; Yamaoka, Y.; Takasu, K.; Yamada, K. *J. Am. Chem. Soc.* **2013**, *135*, 11485. (i) Wanner, B.; Kreituss, I.; Gutierrez, O.; Kozlowski, M. C.; Bode, J. W. *J. Am. Chem. Soc.* **2015**, *137*, 11491. (j) Xu, Y.; Kaneko, K.; Kanai, M.; Shibasaki, M.; Matsunaga, S. *J. Am. Chem. Soc.* **2014**, *136*, 9190. (k) Shinisha, C. B.; Sunoj, R. B. *Org. Lett.* **2009**, *11*, 3242.

(2) (a) Wilent, J. E.; Petersen, K. S. *J. Org. Chem.* **2014**, *79*, 2303. (b) Cheng, Y. A.; Yu, W. Z.; Yeung, Y.-Y. *Org. Biomol. Chem.* **2014**, *12*, 2333.

(3) Qabaja, G.; Wilent, J. E.; Benavides, A. R.; Bullard, G. E.; Petersen, K. S. *Org. Lett.* **2013**, *15*, 1266.

(4) (a) Seguin, T. J.; Wheeler, S. E. *ACS Catal.* **2016**, *6*, 2681. (b) Parmar, D.; Sugiono, E.; Raja, S.; Rueping, M. *Chem. Rev.* **2014**, *114*, 9047. (c) Jindal, G.; Sunoj, R. B. *Angew. Chem., Int. Ed.* **2014**, *53*, 4432.

(5) (a) Itoh, J.; Fuchibe, K.; Akiyama, T. *Angew. Chem., Int. Ed.* **2008**, *47*, 4016. (b) Akiyama, T. *Chem. Rev.* **2007**, *107*, 5744. (c) Kanomata, K.; Toda, Y.; Shibata, Y.; Yamanaka, M.; Tsuzuki, S.; Gridnev, I. D.; Terada, M. *Chem. Sci.* **2014**, *5*, 3515. (d) Terada, M.; Komuro, T.; Toda, Y.; Korenaga, T. *J. Am. Chem. Soc.* **2014**, *136*, 7044. (e) Yamanaka, M.; Kondoh, A.; Terada, M. *J. Am. Chem. Soc.* **2015**, *137*, 1048.

(6) (a) Shibata, Y.; Yamanaka, M. *J. Org. Chem.* **2013**, *78*, 3731. (b) Saito, K.; Shibata, Y.; Yamanaka, M.; Akiyama, T. *J. Am. Chem. Soc.* **2013**, *135*, 11740. (c) Mori, K.; Ichikawa, Y.; Kobayashi, M.; Shibata, Y.; Yamanaka, M.; Akiyama, T. *J. Am. Chem. Soc.* **2013**, *135*, 3964. (d) Yamanaka, M.; Itoh, J.; Fuchibe, K.; Akiyama, T. *J. Am. Chem. Soc.* **2007**, *129*, 6756.

(7) (a) All computations were performed using the Gaussian 09 suite of quantum chemical programs. (b) *Gaussian 09*, revision D.01; Frisch, M. J. et al. Gaussian, Inc., Wallingford, CT. 2013. See the Supporting Information for the full citation and more details of computational methods.

(8) More details of the recognition complexes are provided in Tables S1 and S2 and Figure S1 in the Supporting Information.

(9) See Figures S2−S4 and Table S3 in the Supporting Information for additional details on the concerted pathway.

(10) The relative Gibbs free energies of 30 such transition states (Table S4) and Wiberg indices (Figure S5) are provided in the Supporting Information.

(11) See Figure S6 in the Supporting Information for the Gibbs free energy profile.

(12) See the Supporting Information for more details.

(13) See Table S5 in the Supporting Information for the activation strain analysis on the stereocontrolling transition states.

(14) (a) Bader, R. F. W. *Acc. Chem. Res.* **1985**, *18*, 9. (b) Bader, R. F. W. *Chem. Rev.* **1991**, *91*, 893.

(15) (a) All of the noncovalent interactions have been analyzed by AIM, and details are provided in Figure S7 and Table S6 in the Supporting Information.. (b) Manin, A. N.; Voronin, A. P.; Shishkina, A. V.; Vener, M. V.; Churakov, A. V.; Perlovich, G. L. *J. Phys. Chem. B* **2015**, *119*, 10466. (c) Das, D.; Choudhury, S. R.; Dey, B.; Yalamanchili, S. K.; Helliwell, M.; Gamez, P.; Mukhopadhyay, S.; Estarellas, C.; Frontera, A. *J. Phys. Chem. B* **2010**, *114*, 4998.

(16) (a) Sunoj, R. B. *Acc. Chem. Res.* **2016**, *49*, 1019. (b) Wheeler, S. E.; Seguin, T. J.; Guan, Y.; Doney, A. C. *Acc. Chem. Res.* **2016**, *49*, 1061. (c) Allen, S. E.; Mahatthananchai, J.; Bode, J. W.; Kozlowski, M. C. *J. Am. Chem. Soc.* **2012**, *134*, 12098. (d) Krenske, E. H.; Houk, K. N. *Acc. Chem. Res.* **2013**, *46*, 979.

(17) Johnson, E. R.; Keinan, S.; Mori-Sanchez, P.; Contreras-Garcia, J.; Cohen, A. J.; Yang, W. T. *J. Am. Chem. Soc.* **2010**, *132*, 6498.

(18) See Figures S8 and S9 in the Supporting Information.

DOI: 10.1021/acs.orglett.6b01752
Org. Lett. 2016, 18, 3730−3733